Local wind speed estimation, with application to wake impingement detection

C.L. Bottasso[a,b,*], S. Cacciola[a], J. Schreiber[a]

[a] *Wind Energy Institute, Technische Universität München, Boltzmannstraße 15, D-85748 Garching bei München, Germany*
[b] *Dipartimento di Scienze e Tecnologie Aerospaziali, Politecnico di Milano, Via La Masa 34, I-20156 Milano, Italy*

Abstract

Wind condition awareness is an important factor to maximize power extraction, reduce fatigue loading and increase the power quality of wind turbines and wind power plants. This paper presents a new method for wind speed estimation based on blade load measurements. Starting from the definition of a cone coefficient, which captures the collective zeroth-harmonic of the out-of-plane blade bending moment, a rotor-effective wind speed estimator is introduced. The proposed observer exhibits a performance similar to the well known torque balance estimator. However, while the latter only measures the average wind speed over the whole rotor disk, the proposed approach can also be applied locally, resulting in estimates of the wind speed in different regions of the rotor disk. In the present work, the proposed method is used to estimate the average wind speed over four rotor quadrants. The top and bottom quadrants are used for estimating the vertical shear profile, while the two lateral ones for detecting the presence of a wake shed by an upstream wind turbine. The resulting wake detector can find applicability in wind farm control, by indicating on which side of the rotor the upstream wake is impinging. The new approach is demonstrated with the help of field test data, as well as simulations performed with high-fidelity aeroservoelastic models.

Keywords: Rotor-effective wind speed, wind speed estimation, wakes, wake detection, wind farm control

Notation

A	Rotor disk area
A_B	Planform area of the rotor blade
A_S	Area of a rotor sector
B	Number of blades
C_{m_0}	Cone coefficient
C_P	Power coefficient
D	Rotor diameter
$E(\cdot)$	Expected value
J	Rotor inertia

*Corresponding author, *Tel.:* +49-89-289-16680; *Fax:* +49-89-289-16611.
Email address: carlo.bottasso@tum.de (C.L. Bottasso)

P	Measurement noise variance
Q	Process noise variance
R	Rotor radius
T_{aero}	Aerodynamic torque
T_{friction}	Friction torque
T_{gen}	Generator torque
V	Wind speed
m	Out-of-plane bending moment
n	Gearbox ratio
q	Dynamic pressure
r	Spanwise radial coordinate
t	Time
u	Longitudinal wind speed
v	Measurement noise
w	Process noise
z	Kalman filter output
Ω	Rotor speed
β	Blade pitch angle
δ_{TI}	Left-right relative turbulence intensity difference
δ_{V}	Left-right relative wind speed difference
ϵ	Error
γ	Horizontal wind misalignment
κ	Vertical power-law shear exponent
κ_{lin}	Vertical linear shear coefficient
λ	Tip speed ratio
ψ	Azimuth angle
ρ	Air density
σ	Standard deviation
ξ	Non-dimensional spanwise radial coordinate
$\bar{(\cdot)}$	Average quantity
$\dot{(\cdot)}$	Time derivative, $\mathrm{d}\cdot/\mathrm{d}t$
$\hat{(\cdot)}$	Measured quantity
$(\cdot)_{\text{BE}}$	Blade-effective quantity
$(\cdot)_{\text{RE}}$	Rotor-effective quantity

$(\cdot)_{\mathrm{SE}}$	Sector-effective quantity
$(\cdot)_h$	Quantity referred to the hub
$(\cdot)_i$	Quantity referred to the ith blade
$(\cdot)_k$	Quantity referred to the kth time step
BEM	Blade Element Momentum
BLE	Blade Load Estimator
HAWT	Horizontal Axis Wind Turbine
ILS	Integral Length Scale
LiDAR	Light Detection And Ranging
REILS	Rotor-Effective Integral Length Scale
RETI	Rotor-Effective Turbulence Intensity
REWS	Rotor-Effective Wind Speed
SETI	Sector-Effective Turbulence Intensity
SEWS	Sector-Effective Wind Speed
TBE	Torque Balance Estimator
TI	Turbulence Intensity
TSR	Tip Speed Ratio

1. Introduction

Modern wind power plants may contain tens or hundreds of individual wind turbines. Each machine converts into electrical energy a part of the kinetic energy carried by an air stream tube interacting with its rotor disk. As a consequence of this energy conversion process, behind each wind turbine a complex wake structure develops, which is characterized by a slower wind speed and a higher turbulence intensity. Wakes undergo complicated phenomena, including the breakdown of near-rotor vortical structures, mixing, recovery, meandering and merging with other wakes. All such processes are strongly influenced by several parameters, including the operating conditions of the machines, the characteristics of the atmosphere, the orography and roughness of the terrain or the sea state, and the interactions among neighboring wakes.

Wakes impinging on downstream wind turbines within a wind farm are a cause of significant power losses and increased fatigue loading. Several solutions to address this problem are currently being actively investigated [1], including the idea of redirecting wakes away from downstream machines [2, 3, 4, 5], the curtailment of power of upstream wind turbines [6], the promotion of a faster wake recovery —for example by pitching the rotor blades [7]—, and the alleviation of loads on the affected downstream machines by active controls [8].

For developing effective solutions that are capable of actively changing the wind farm flow, a precise knowledge of the wind inflow conditions at the rotor disk of each machine is essential. For example, when using wake redirection to alleviate a partial wake overlap, it is necessary to know with certainty which side of the downstream rotor is affected, in order to deflect the wake of the upstream machine in the correct direction.

Unfortunately, at present wind turbines do not operate based on a detailed understanding of the wind conditions that affect them. In fact, wind turbines typically use nacelle or hub mounted wind measurement devices, which can only provide information on wind speed and direction at the single point in space where these devices are installed. Therefore, wind turbines are unaware of the presence of an impinging wake and of many other important inflow parameters, as for example vertical shear and veer. Clearly, this lack of situation awareness severely limits the application of sophisticated wind turbine and wind farm control approaches.

Reduced wind farm models [9, 10], often based on engineering wake models or model-compression techniques, are able to represent to a certain extent the wind farm flow conditions and wake interactions at a moderate computational complexity. Given their limited computational cost, such models are also good candidates for the synthesis of model-based controllers. However, the quality and reliability of the predictions provided by these models are typically affected by a number of factors, including the stability and characteristics of the atmosphere and the proper calibration of the model parameters. Even in this case, a more sophisticated awareness of the flow conditions than it is currently available would prove very valuable. If one could measure the wind conditions at the rotor disk of each machine, this information could be used to improve/correct the predictions of the reduced order models, in turn providing higher quality information for advanced control applications.

LiDARs (Light Detection And Ranging) are remote sensing devices that are able to measure wind conditions and to detect wakes and their locations [11]. Both ground-based and nacelle-mounted LiDARs, possibly used in synergy, can provide a fairly complete description of the flow at the sampling rates necessary for wind turbine and wind farm control. Unfortunately, however, the use of LiDARs is still confined to research applications, and they are not yet routinely deployed in the field on production machines because of cost, availability, reliability and technological limits of the measurements. These include spatio-temporal averaging, complexity of multi-component measurements of the wind vector, effects of turbulence convection and interaction with the rotor induction zone.

In summary, there is a need to develop alternative methods for wind flow measurement that can improve the situation awareness of wind turbines. Such methods should be simple and reliable, and they should be able to provide detailed information on the flow characteristics at each wind turbine rotor disk in real time during operation. The availability of such new methods would facilitate the development of modern smart control approaches, to improve power capture and reduce loading for wind turbines operating within power

plants.

To address these needs, the concept of using the rotor as a generalized anemometer has been recently proposed [12, 13, 14, 15]. In a nutshell, the idea of *wind sensing* is that any change in the wind conditions at the inflow will be reflected in a corresponding change in the response of the rotor. In other words, there is in general a well defined map between some wind parameters and some specific features of the rotor response. By measuring such response —for example in terms of blade loads or accelerations, torque, rotor speed, blade pitch, etc.— one may invert the map, under suitable hypotheses and conditions, to estimate the wind characteristics. Recent results (see [15] and references therein) indicate that several wind states can be reliably observed using blade loads, including wind speed, vertical and horizontal shears, lateral misalignment and upflow. As many modern machines are already equipped with load sensors, typically for enabling load-alleviating feedback control laws, the implementation of such approaches may not require any additional hardware, and therefore may come at the cost of a simple software upgrade.

The current paper falls within the new field of wind sensing. Within the general idea of using the rotor as a wind sensor, the present work proposes a new and simple method to estimate some wind characteristics that imply non-uniform wind conditions at the rotor disk. Relevant examples are vertical shear and the impingement of a wake shed by an upstream machine.

The method is based on the estimation of the wind speed by the out-of-plane blade bending moment, as explained in more detail in Section 2. Similarly to the thrust coefficient, one may define a cone bending coefficient, which depends on the tip speed ratio (TSR) and blade pitch. The cone coefficient captures the (collective) zeroth-harmonic of the blade loads, and it can be interpreted as the constant term produced by Coleman-transforming the individual loads of each blade. Using the three blades together, knowledge of the loads in addition to rotor speed and blade pitch allows one to estimate a rotor-equivalent wind speed from the cone coefficient. The estimate is obtained by the use of a Kalman filter, which enhances the robustness of the approach in the face of noise and disturbances, always present in practical applications in the field.

A similar rotor-equivalent estimate of the wind speed may be obtained by the well known torque balance estimator [12]. In that case, one uses the power coefficient and, based on measured shaft torque together with rotor speed and blade pitch, wind speed is obtained by filtering. A comparison between the two approaches shows results of similar quality. It is speculated that the present approach might yield better estimates in the high frequency spectrum, especially on machines with particularly large diameters. In fact, the flap response of the rotor is not slowed by its large rotary inertia, as it is on the other hand the case for the torque balance estimator. Results shown in this paper indicate that the method has sufficient temporal resolution for estimating with good accuracy even the Turbulence Intensity (TI), and in turn the Integral Length Scale (ILS) of the flow.

However, a crucial difference of the proposed approach with respect to the torque balance method is

that the former can be specialized to the observation of *local* flow conditions on different parts of the rotor; this is in contrast to the exclusively *global* estimates provided by the latter. Specifically, by using the load information for each single blade independently, one may sense the wind at the azimuthal location occupied by that blade, as explained in Section 3. Averaging over an azimuthal interval, an estimate of the local wind speed in a rotor sector can be readily obtained. In turn, from the local wind speed one may also easily derive an estimate of the corresponding local TI.

This new idea is here developed by subdividing the rotor into four quadrants, although other choices are clearly possible. The local speed estimates obtained by the proposed method may be used to detect speed differences over the rotor disk. At first, the idea of detecting the effects of the vertical shear is investigated by using field test data. Experiments conducted with different data sets show that the vertical distribution of wind speed detected over the top and bottom rotor quadrants correlates well with the one measured by a met-mast equipped with anemometers.

In Section 4, the new proposed concept is finally applied to the observation of waked conditions. A simulation environment is used in this case. Although any model cannot clearly be perfectly faithful to reality, the use of simulations has the advantage that one has a complete knowledge of the situation. In the present case, this means that one knows exactly the ground truth wind speeds in the various areas of interest. In addition, it is easier within a simulation environment to try and determine the effects of various disturbing effects. The study considers various waked conditions, which differ in the degree of overlap with the affected rotor disk. Extensive simulations and comparisons of the results of the observations with respect to the reference exact solutions demonstrate the general ability of the proposed formulation of distinguishing between waked and unwaked conditions, indicating the affected rotor side of the interaction. Other recent related papers [16, 17, 18] present studies of the performance of the same method with reference to experimental data measured on a scaled wind farm facility. The papers also show how to estimate the wake position based on the local wind speed estimates developed in the present work.

Finally, the present work is terminated by Section 5, where conclusion are drawn and plans for future work are sketched.

2. Estimation of rotor-effective wind parameters

2.1. A novel formulation for wind speed estimation based on the cone coefficient

In this work, the Rotor-Effective Wind Speed (REWS) is obtained by a Blade-Load-based Estimator (BLE), which makes use of the zeroth harmonic (or cone) of the out-of-plane bending rotor loads. Considering a steady wind condition, the cone coefficient is defined as

$$C_{\mathrm{m}_0}(\lambda_{\mathrm{RE}}, \beta, q_{\mathrm{RE}}) = \frac{\frac{1}{2\pi}\int_0^{2\pi}\sum_{i=0}^{B} m_i(\psi_i)\mathrm{d}\psi}{\frac{1}{2}\rho A R V_{\mathrm{RE}}^2}, \tag{1}$$

where $\lambda_{\mathrm{RE}} = \Omega R / V_{\mathrm{RE}}$ is the rotor-effective TSR, Ω the rotor speed, R the rotor radius, V_{RE} the REWS, β the blade pitch angle, B the number of blades, m_i the out-of-plane root bending moment of blade i (which occupies the azimuthal position ψ_i over the rotor disk), ρ the density of air, A the rotor disk area and finally $q_{\mathrm{RE}} = 1/2 \rho V_{\mathrm{RE}}^2$ the rotor-effective dynamic pressure. The numerator of the right hand side represents the average over a rotor revolution of the sum of the out-of-plane blade bending moments, $m_0 = \sum_{i=1}^{B} m_i$. In the terminology of the Coleman transformation, m_0 represents the collective, cone or zeroth harmonic of the loads, while the higher harmonics would be given by appropriate sine and cosine combinations of the same loads [19].

As in the case of the familiar power and thrust coefficients, also the cone coefficient depends on the operating condition through TSR and blade pitch. In addition, as indicated on the left hand side of the previous expression, the cone coefficient also depends on dynamic pressure. In fact, rotor and tower deform under loading, so that the same TSR and blade pitch at two different wind and/or density conditions may in principle correspond to slightly different non-dimensional cone (but also power and thrust) coefficients.

Once the cone coefficient has been computed for all operating conditions of interest, Eq. (1) can be used to estimate V_{RE}. To this end, the equation is rewritten for the generic time instant t as

$$\hat{m}_0(t) = \frac{1}{2} \rho A R V_{\mathrm{RE}}^2(t) C_{\mathrm{m_0}}\big(\lambda_{\mathrm{RE}}(t), \beta(t), \bar{q}_{\mathrm{RE}}(t)\big), \tag{2}$$

where $\hat{m}_0$ is computed based on the measurements provided at that instant of time by blade load sensors. The rotor-effective dynamic pressure $\bar{q}_{\mathrm{RE}}$ is computed by a moving average looking backward in time over a suitable time window, to capture the working point about which the machine is operating. Since also the rotor speed Ω can be easily measured together with the blade pitch angle β, the sole unknown in the equation is the REWS V_{RE}, which can therefore be readily computed.

The contribution of the gravitational loads are assumed to have been eliminated from the blade bending moments. In fact, not having an aerodynamic origin, gravitational loads cannot be non-dimensionalized by the denominator of Eq. (1). In turn, this prevents the correction of the coefficient for density, which is on the other hand important for the practical application of the method in realistic conditions. The elimination of the effects of gravity is achieved by first pre-computing the corresponding bending moments for preselected values of the azimuthal blade position, at each time step interpolating these values to get the one corresponding to the actual position, and finally subtracting the interpolated value from the currently measured bending moment. As previously noted, to account for the deformation of the machine at different operating points, such procedure can be scheduled in terms of the current mean dynamic pressure.

To increase the robustness of the estimates in the face of measurement and process noise, an Extended Kalman filter is used for the computation of V_{RE}. The wind speed update at the generic time step k is defined

as

$$V_{\mathrm{RE}_k} = V_{\mathrm{RE}_{k-1}} + w_{k-1}, \tag{3}$$

w_k being the process noise with covariance Q. The very simple model used here has the advantage of depending on the single tuning parameter Q, and it performed reasonably well in the experiments reported later on. Nonetheless, it is clear that a more sophisticated model of the wind dynamics might be considered, for example in order to ensure specific characteristics to the wind spectrum. Finally, the non-linear output equation of the filter is defined as

$$z_k = \frac{1}{2}\rho A R V_{\mathrm{RE_k}}^2 C_{\mathrm{m_0}}(\lambda_{\mathrm{RE}}, \beta, \bar{q}_{\mathrm{RE}_k}) - m_0 + v_k, \tag{4}$$

where v_k is the measurement noise with covariance P, while the output z_k is set to 0 to enforce Eq. (2) at each step. The filter parameters Q and P should be tuned in order to obtain good quality estimates in different wind conditions, as shown later on in the results section.

2.2. Estimation of wind speed by the power coefficient

A dynamic Torque Balance Estimator (TBE) [12, 20, 21, 22, 23] of the REWS is described next. The well known TBE is introduced to provide a reference performance in the estimation of the wind speed, to be used for comparison and validation of the previously described cone-coefficient-based estimator. The TBE uses a dynamic model of the rotor torque balance, which writes

$$J\dot{\Omega} = T_{\mathrm{aero}} - nT_{\mathrm{gen}} - T_{\mathrm{friction}}, \tag{5}$$

where J is the moment of inertia of the rotor-generator-drive-train assembly referred to the low speed shaft, $\dot{\Omega}$ the rotor acceleration, T_{aero} the aerodynamic torque, n the gearbox ratio, T_{gen} the generator torque and $T_{\mathrm{friction}}(\Omega)$ a mechanical loss term accounting for friction in the bearings and drive-train. The aerodynamic torque can be expressed as a function of the power coefficient C_P as

$$T_{\mathrm{aero}} = \frac{1}{2\Omega}\rho A V_{\mathrm{RE}}^3 C_{\mathrm{P}}(\lambda_{\mathrm{RE}}, \beta, q_{\mathrm{RE}}). \tag{6}$$

Note that the power coefficient, similarly to the cone coefficient, is a function of the dynamic pressure as it may be influenced by aeroelastic effects. Here again, as all quantities appearing in the equation are either measured or can be estimated, the sole remaining unknown is the REWS V_{RE} for which the equation can be solved.

Even in this case, to hedge against disturbances and noise the Extended Kalman filter is used, resulting in the following non-linear output equation

$$z_k = \frac{1}{2\Omega}\rho A V_{\mathrm{RE_k}}^3 C_{\mathrm{P}}(\lambda_{\mathrm{RE}}, \beta, \bar{q}_{\mathrm{RE}_k}) - nT_{\mathrm{gen}} - T_{\mathrm{friction}} - J\dot{\Omega} + v_k. \tag{7}$$

2.3. Estimation of turbulence intensity and integral length scale

The Rotor-Effective Turbulence Intensity (RETI, noted TI_{RE}) is directly obtained by the 10-minute REWS mean $\bar{V}_{\mathrm{RE}}$ and standard deviation $\sigma_{V_{\mathrm{RE}}}$:

$$TI_{\mathrm{RE}} = \frac{\sigma_{V_{\mathrm{RE}}}}{\bar{V}_{\mathrm{RE}}}. \tag{8}$$

Clearly, for the RETI to be a good quality estimate of the real flow turbulence intensity interacting with the rotor disk, the REWS should approximate the real wind speed in a sufficiently ample bandwidth, typically up to 0.2 Hz. In this sense, REWS estimators that perform an excessive filtering effect might not provide for suitable estimates of the RETI.

The Rotor-Effective Integral Length Scale (REILS) is readily obtained based on the 10-minute auto-correlation of the REWS, as for example described in Ref. [24].

2.4. Comparison of the two methods

Before moving on to the estimation of local wind speeds, estimates of rotor-equivalent wind quantities based on blade loads are compared to the ones obtained with the use of the well known TBE, with the purpose of establishing the performance characteristics of the new method.

At first, a simulation study was conducted by using the high-fidelity aeroservoelastic model of a 3 MW wind turbine, implemented with the modeling environment `Cp-Lambda` [25]. The machine is an upwind three-bladed variable-speed HAWT, representative of current wind turbine designs, with a rotor diameter of 93 m and a hub height of 80 m. The wind turbine is modelled as a flexible multibody system expressed in Cartesian coordinates, whose blades and tower are rendered using geometrically exact beam models, which are in turn discretized in space using the isoparametric finite element method. Lagrange multipliers are used for enforcing mechanical constraints, resulting in a high-index differential algebraic formulation, which is marched in time by a preconditioned energy decaying integration scheme [26]. The aerodynamic model is based on the coupling of lifting lines with the classical Blade Element Momentum (BEM) theory. The model operates in closed-loop with a collective blade pitch and torque controller. Turbulent wind fields were obtained with the `TurbSim` code [27]. At each instant of time, sensors within the model, including strain sensors at the blade roots emulating strain-gages, gather the necessary information that is in turn fed to the estimators.

At each time instant, a reference "ground-truth" REWS was calculated from the wind grid as

$$V_{\mathrm{RE,grid}} = \frac{1}{A}\int_0^{2\pi}\int_0^{R} u(r,\psi) r \,\mathrm{d}r \,\mathrm{d}\psi, \tag{9}$$

where u is the wind speed in the longitudinal direction, similarly to what done by Østergaard et al. [20]. Other definitions are possible, as the one used by Soltani et al. [12], where wind speed is weighted by the

local power coefficient. Based on this reference REWS, reference RETI and REILS were readily obtained, as previously described.

Figure 1a shows at top the reference REWS (at left) and RETI (at right), for parts of one turbulent wind realization characterized by an ambient wind speed of 20 m/s with a TI of 5% and a vertical layer with shear exponent equal to 0.2, based on the Kaimal turbulence model. The bottom part of the figure shows the corresponding errors between estimate and reference, for both the REWS (at left, in meters per second) and the RETI (at right, in percentage points).

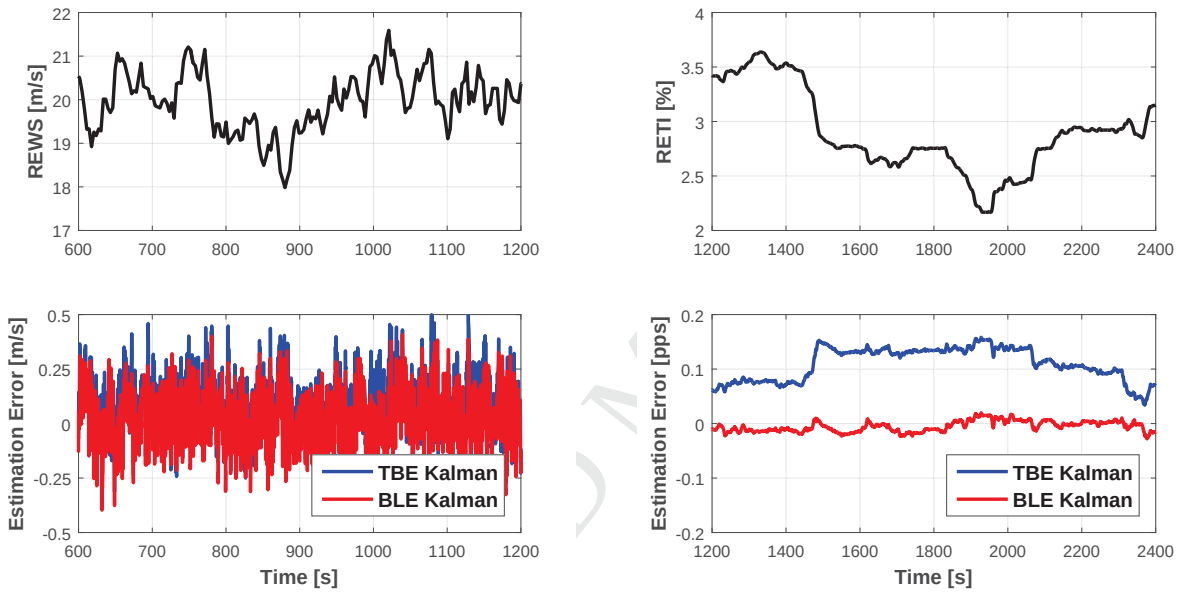

(a) REWS (b) RETI

Figure 1: Top: reference REWS (at left) and RETI (at right). Bottom: estimation errors for REWS (at left) and RETI (at right).

For different average wind speeds and TIs, the estimation error mean $E[\epsilon]$ and standard deviation σ_ϵ are shown in Table 1a. These quantities are computed on one realization of the turbulent wind time history of 40 minutes of length, which are enough to bring the statistics to convergence. Results indicate that both methods produce similarly good estimates.

For the same wind conditions, Table 2 reports the statistical properties of the estimation error for the REILS, in percentage. Again both estimators yield reliable results, although the TBE appears to be slightly more accurate.

Next, field measurements were used to characterize the quality of the BLE, again in comparison with the TBE. Measurements were obtained on the CART3 (Controls Advanced Research Turbine, 3-bladed) [28],

ambient		$E[\epsilon]$ in m/s		σ_ϵ in m/s	
V	TI	BLE	TBE	BLE	TBE
5m/s	2%	-0.03	-0.03	0.02	0.01
5m/s	5%	-0.04	-0.03	0.03	0.02
5m/s	10%	-0.05	-0.02	0.05	0.05
20m/s	2%	0.02	0.07	0.06	0.07
20m/s	5%	0.02	0.08	0.13	0.14
20m/s	10%	-0.09	0.02	0.25	0.25

(a) REWS

ambient		$E[\epsilon]$ in pps		σ_ϵ in pps	
V	TI	BLE	TBE	BLE	TBE
5m/s	2%	0.14	-0.02	0.07	0.01
5m/s	5%	0.12	-0.04	0.17	0.03
5m/s	10%	0.10	-0.10	0.28	0.05
20m/s	2%	0.06	0.13	0.01	0.01
20m/s	5%	-0.01	0.11	0.01	0.03
20m/s	10%	-0.03	0.05	0.03	0.04

(b) RETI

Table 1: REWS and RETI estimation error means $E[\epsilon]$ and standard deviations σ_ϵ for the BLE and TBE estimators, for multiple realizations of different wind conditions.

ambient		$E[\epsilon]$ in %		σ_ϵ in %	
V	TI	BLE	TBE	BLE	TBE
5m/s	2%	0.94	3.82	5.29	3.10
5m/s	5%	5.49	5.08	5.36	5.21
5m/s	10%	5.56	5.12	4.66	4.58
20m/s	2%	0.16	-0.82	9.96	6.00
20m/s	5%	2.56	0.33	6.51	5.93
20m/s	10%	1.81	0.47	5.79	4.72

Table 2: REILS estimation error means $E[\epsilon]$ and standard deviations σ_ϵ for the BLE and TBE estimators, for multiple realizations of different wind conditions.

operated by the National Wind Technology Center (NWTC) of the National Renewable Energy Laboratory (NREL). This 600 kW wind turbine has a rotor radius of 20 m and a hub-height of 40 m.

A met-mast is located 85 m from the wind turbine, and it is equipped with three anemometers and wind vanes located at 15, 36 and 55 m above ground. Wind recordings sampled at 400 Hz were selected for wind directions aligned with the met-mast and wind turbine axis. To account for the time delay between met-mast and wind turbine, the three anemometer measurements were first averaged at each time instant to give a rotor mean wind speed, and then time-shifted based on the 1500-second averaged mean wind speed.

The wind turbine cone and power coefficients were based on a previously validated aeroelastic model of the wind turbine, implemented with the simulation tool `FAST` [29, 30]. The coefficients were obtained by averaging the machine relevant response obtained with dynamic simulations in steady-state winds at various TSR and blade pitch settings, once the solution had settled onto a periodic orbit. Given its small size and robust construction, for this machine the dependency of the coefficients on the dynamic pressure is negligible, and therefore it was not taken into account.

For one specific representative time history of 600 s of duration, Fig. 2 shows the met-mast average, as well as the REWS computed by the BLE and the TBE. For completeness, the plot also reports the wind speed measured by the nacelle-mounted anemometer, which however is a point measurement (as opposed to a rotor-equivalent quantity) and also exhibits a significant offset. It should be mentioned that in this case the met-mast-measured wind can hardly be considered as a "ground truth", as it is only based on three point measurements and it neglects the evolution of the flow from the met-mast to the wind turbine rotor (Taylor's frozen hypothesis). Nonetheless, the plot shows that the BLE and TBE are in good agreement between themselves and in a reasonable one with the met-mast-provided information. Similar results were obtained with the use of different time histories from this same machine and experimental setup.

3. Estimation of local-effective wind parameters

The BLE method can be finally specialized to estimate the wind speed experienced in different parts of the rotor disk. The basic idea is to use each blade as a moving sensor whose out-of-plane bending load is strictly connected to the local wind speed at the blade position.

To this end, Eq. (2) is modified as

$$\hat{m}_i(t) = \frac{1}{2B}\rho A R V_{\mathrm{BE}}\big(\psi_i(t)\big)^2 C_{\mathrm{m}_0}\Big(\lambda_{\mathrm{BE}}\big(\psi_i(t)\big), \beta_i, q_{\mathrm{BE}}\Big), \tag{10}$$

where $(\cdot)_i$ indicates quantities pertaining to the ith blade. As in the previous case, this expression is used to define the output equation of an Extended Kalman filter (cf. Eq. (4)), which yields an estimate of the blade local-effective wind speed $V_{\mathrm{BE}}(\psi_i(t_k))$ at the azimuthal location ψ_i occupied by the blade at time instant t_k.

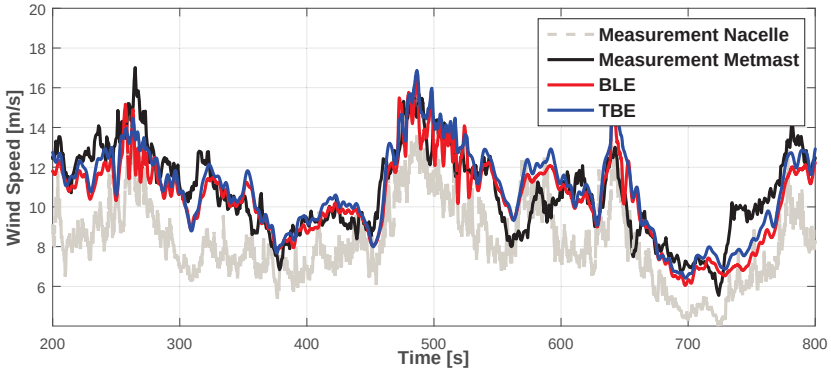

Figure 2: REWS BLE (red line) and TBE (blue line) estimates, averaged time-shifted met-mast wind speed (black line), and onboard nacelle-mounted anemometer wind speed (gray dashed line), for field measurements obtained with the NREL CART3 wind turbine.

From the blade local-effective wind speed, a Sector-Effective Wind Speed (SEWS), noted V_{SE}, is obtained by averaging over an azimuthal interval of interest, as

$$V_{\mathrm{SE}}(t) = \frac{1}{A_{\mathrm{S}}} \int_{A_{\mathrm{S}}} V_{\mathrm{BE}}(\psi(t))\, \mathrm{d}A_{\mathrm{S}}. \tag{11}$$

The SEWS estimate can be updated every time a blade leaves the sector, i.e. with a frequency equal to $B\times$Rev, while the zero-order hold can be employed in between two updates. This concept is symbolically illustrated in Fig. 3.

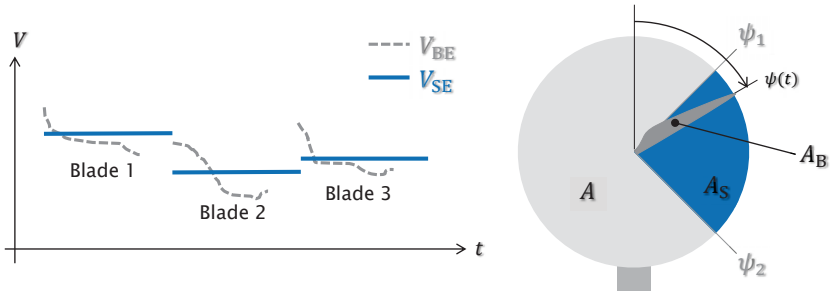

Figure 3: Estimation of blade-effective and sector-effective wind speeds, from the loads of a blade passing through a rotor disk sector.

A Sector-Effective Turbulence Intensity (SETI), noted TI_{SE}, is readily computed from the SEWS as

$$TI_{\mathrm{SE}} = \frac{\sigma_{V_{\mathrm{SE}}}}{\bar{V}_{\mathrm{SE}}}, \tag{12}$$

being $\sigma_{V_{\mathrm{SE}}}$ the standard deviation of the SEWS.

The SEWS has the meaning of an average velocity over the disk sector. Hence, the question arises: what is the spanwise location of such an average along the disk radius? In fact, this information may be useful for the validation and interpretation of the results. For example, later on the estimated SEWS will be compared to measurements obtained with a met-mast, and therefore it is necessary to know at which height along the met mast the comparison should be performed.

The blade root bending moment on a sector S occupying the azimuthal span $\Delta\psi = \psi_2 - \psi_1$ with area $A_{\mathrm{S}} = \Delta\psi R^2/2$ can be written as

$$m_{\mathrm{S}} = \frac{1}{2B}\rho R^3 \int_0^1 \int_{\psi_1}^{\psi_2} V(\xi,\psi)^2 C_T(\xi,\psi)\xi^2 \,\mathrm{d}\psi\mathrm{d}\xi, \tag{13}$$

where $\xi = r/R$ is the nondimensional radial position, r the dimensional one, and C_T the local thrust coefficient. According to stream-tube theory, $C_T(\xi) = 4a(\xi)\big(1 - a(\xi)\big)$, where $a(\xi)$ is the axial induction factor. As $a(\xi) \approx 1/3$ for a well designed blade, then C_T can be assumed to be roughly constant over the rotor disk. Therefore, introducing the constant equivalent wind speed V_{SE} over the sector, one readily finds

$$m_{\mathrm{S}} = \frac{1}{2B}\rho V_{\mathrm{SE}}^2 A_{\mathrm{S}} \frac{2}{3} R C_T. \tag{14}$$

This expression indicates that the blade bending moment can be interpreted as being produced by the thrust applied at $2R/3$ span. In this sense, V_{SE} can be interpreted as the wind velocity sampled at that same location.

A more refined analysis can be developed by assuming a linear vertical wind shear, which can be expressed as

$$V(\xi,\psi) = V_h\left(1 + \kappa_{\mathrm{lin}}\frac{z - z_h}{R}\right), \tag{15a}$$

$$= V_h(1 + \kappa_{\mathrm{lin}}\,\xi\cos\psi), \tag{15b}$$

where V_h is the hub height, κ_{lin} the linear shear coefficient, and z a vertical coordinate pointing upwards, z_h being the hub height. In this case, one would like to find the equivalent height $\tilde{z}$ where V is sampled by the estimator. Using both expressions (15a) and (15b) in Eq. (13), considering a constant C_T, solving for z and simplifying the result, one finds the following expression for the effective height $\tilde{z}$:

$$\frac{\tilde{z} - z_h}{R} = \frac{1}{\kappa_{\mathrm{lin}}}\left(\sqrt{\frac{\int_0^1\int_{\psi_1}^{\psi_2}(1 + \kappa_{\mathrm{lin}}\,\xi\cos\psi)^2\xi^2\,\mathrm{d}\psi\mathrm{d}\xi}{\Delta\psi/3}} - 1\right). \tag{16}$$

Even though the effective height is a function of the shear coefficient κ_{lin}, one may safely assume $(\tilde{z}-z_h)/R \approx \pm 2/3$ for the upper and lower sectors. Indeed, the variation of this quantity with κ_{lin} is very small, being for the upper sector $(\tilde{z}-z_h)/R|_{\kappa_{\text{lin}}=-0.5} = 0.662$ and $(\tilde{z}-z_h)/R|_{\kappa_{\text{lin}}=+0.5} = 0.682$.

3.1. Use of local-effective wind parameters

The concept of SEWS can be used for detecting areas of different wind speeds over the rotor disk. For example, consider the four quadrants depicted in Fig. 4.

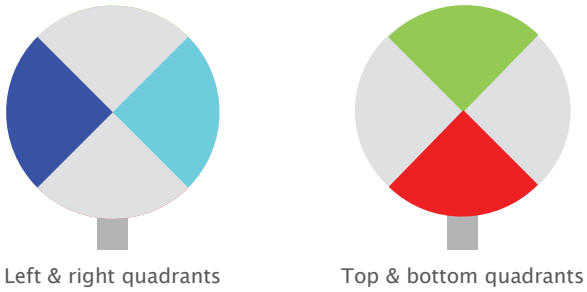

Figure 4: Rotor disk partitioned into four quadrants, noted left and right, and top and bottom. Naming of the quadrants considers an upwind view direction.

A partial wake impingement, whereby the wake shed by an upstream wind turbine has a partial overlap with the rotor disk, will create different wind speeds on the right and left sectors of the rotor. Therefore, by looking at the difference of the SEWS between the right and left quadrants, one may be able to detect a wake interference condition, information that can be exploited for wind farm control. This information can also help distinguish whether the wake is impinging over one or the other side of the rotor disk, which is again useful for wake redirection control purposes.

Since a wake is characterized not only by a speed deficit but also by a higher TI than the ambient flow, a partial wake condition will also typically imply different TI levels on the two sides of the rotor. As the proposed formulation is also capable of estimating local TI values over the different quadrants, this information can in principle be used in conjunction with the local speed to increase the confidence level of a correct wake interference detection.

Similarly, a vertical wind shear will imply different wind speeds on the top and bottom quadrants. Here again, the SEWS on these two rotor sectors may be used for estimating this wind parameter, which in turn may find applicability in wind turbine and wind farm control (for example, by correlating wind shear and atmospheric stability, which has strong effects on the behavior of wakes). Additionally, by averaging over

the left and right quadrants, one may have an indication of the wind speed at hub height. This, together with the SEWS of the top and bottom quadrants, produces a three-point estimate of the wind speed in the vertical direction, which can in principle be used for estimating an inverted wind profile, typical of conditions characterized by low level jets. In this case, the use of a higher number of sectors than the four used here might provide for an even better vertical resolution.

The use of SEWS for estimating shear and wake impingement is demonstrated in the following pages by the use of several examples, which make use of synthetic simulation data as well as field tests. A validation performed with scaled experiments conducted with wind turbine models in a boundary layer wind tunnel is described in a different publication [16].

4. Results

4.1. Vertical shear estimation from field test data

At first, the proposed formulation was verified with respect to its ability in estimating the vertical wind shear, again with reference to field test data gathered on the NREL CART3 wind turbine. Although the primary goal of this work is the development of a wake state estimator, both vertical shear and wake interference are characterized by different average wind speeds on different rotor quadrants. Therefore, this test still gives relevant information on the general ability of the formulation of detecting wind speed variations over the rotor disk.

Based on the previously illustrated analysis, wind velocity estimates can be interpreted as flow samples at $2/3R$. Therefore, for the lower sector, estimates are compared to the time-shifted and linearly interpolated anemometer measurements at $2/3R$ below hub height (i.e., 27 m from the ground). Similarly, the upper sector reference is obtained by interpolating the measurements at $2/3R$ above hub height (i.e., 53 m from the ground).

Figure 5 shows a time history of the estimated SEWS for a period of 100 s. It should be noted that the distance between met-mast and wind turbine clearly implies an approximation due to the adoption of Taylor's frozen turbulence hypothesis. In addition, it should also be remarked that the SEWS represents a spatial mean wind speed, while anemometers only provide point-wise measurements. Nonetheless, considering these two limitations of the present comparison, the estimates follow reasonably well the trend of the met-mast anemometers. In particular, it appears that the estimates are capable of consistently detecting the right sign of the shear (in other words, whether the speed in the top quadrant is higher or not than in the lower one), and the correct overall behavior of this quantity.

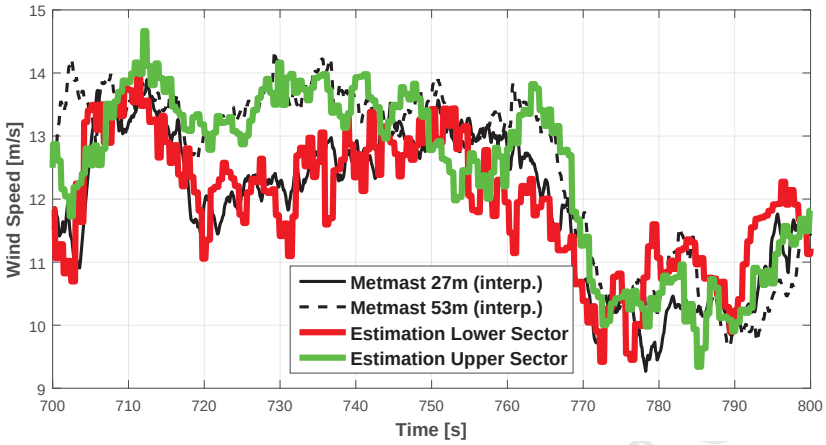

Figure 5: SEWS estimation based on NREL CART3 measurements of the bottom (red) and top (green) sectors. Interpolated and time-shifted met-mast measurements are shown as reference in black.

4.2. Wake state estimation

The simple wind farm layout depicted in Fig. 6 was used for studying the ability of the proposed formulation in detecting the impingement on a rotor of the wake shed by an upstream wind turbine. Both machines are 3 MW HAWTs, identical to the ones used in the previous numerical study.

The longitudinal distance between the two wind turbines is four times the diameter of the rotor (4D), which is a closely spaced configuration that might be representative of compact wind farms designed to reduce land occupation in onshore sites located in geographical areas of relatively high population density. The lateral distance of the two wind turbines is taken as a parameter, which is varied in order to realize different wake overlaps for a given fixed wind direction. When noted, the downstream wind turbine operates with a given misalignment angle γ with respect to the wind vector, which will probably be a relatively common mode of operation in the future within closely spaced wind farms. In fact, deliberate wind misalignment can be used for deflecting the wake away from downstream machines, thereby reducing interferences to the benefit of power output and loading. Tests conducted herein with a misaligned machine are meant to verify whether the wake state observer works also in this operating condition.

The wake of the upwind turbine is modeled by the superposition of a turbulent wind grid generated with `TurbSim`, and the first order solution of the wind speed deficit of the Larsen model (EWTSII model) [31]. Although this is only a rather crude and idealized behavior of a wind turbine wake, it still serves the purpose of generating a wind field that has different wind speed values and TIs over the rotor of the affected downstream wind turbine.

As an example of the wind fields generated this way, Fig. 7a shows for a random time instant the `TurbSim` wind grid obtained for a mean wind speed of 8 m/s, a 5% TI and a shear layer with exponent equal to 0.2.

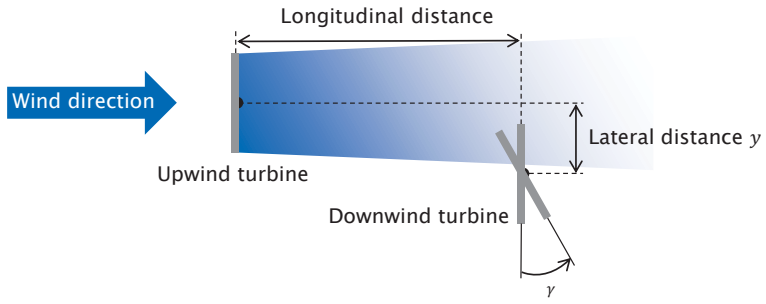

Figure 6: Configuration of the two wind turbines for the wake detection simulation study.

For the same instant of time, Fig. 7b shows the superposition of the turbulent wind with the Larsen model, for a lateral distance between the two machines of 0.5D.

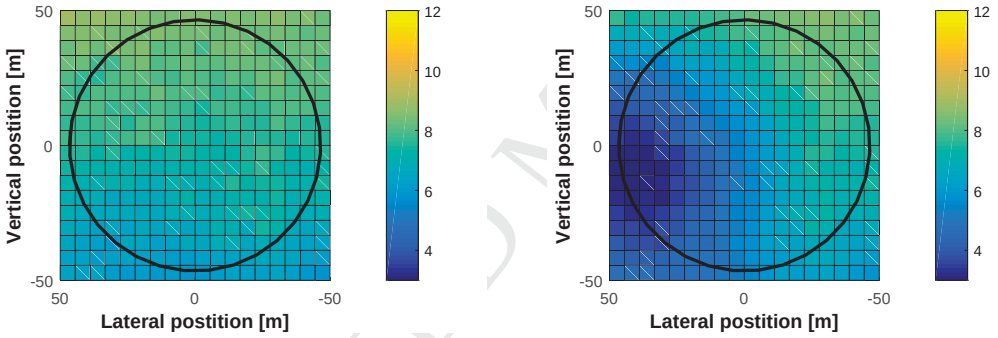

(a) Baseline turbulent wind field (b) Baseline superimposed with Larsen model

Figure 7: Turbulent wake model obtained by the superposition of Kaimal turbulence with Larsen model. Color bar in m/s; the downstream rotor circumference is indicated by a black circle.

Due to the wind speed deficit characterizing the wake core, turbulence inside the wake is increased, as shown in Fig. 8. Figure 8a shows the 10-minute TI in percentage at each grid point without wake superposition, whereas Fig. 8b shows the same quantity for the two superimposed wind fields. Clearly, this is only a very crude model of the actual turbulent behavior of a wake, although here again it serves the purpose of creating areas of different TI over the rotor disk.

4.3. Wake interference detection

There may be multiple ways of detecting a wake impingement by analyzing the turbine response. For a reliable wake detection a combination of various methods may be advisable, including geometric information

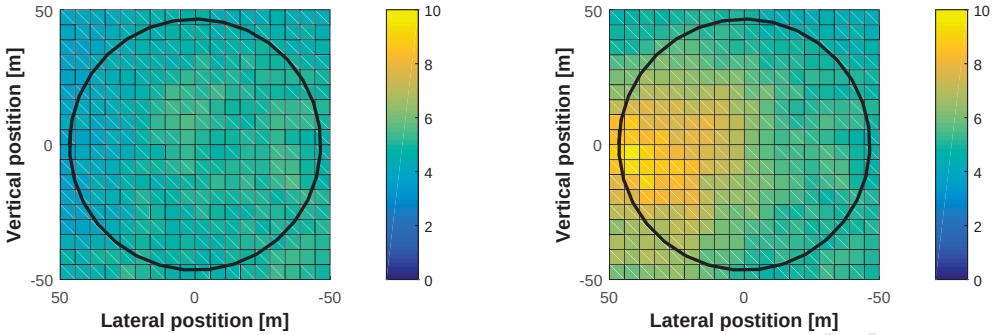

(a) Baseline turbulent wind field

(b) Baseline superimposed with Larsen model

Figure 8: TI for the turbulent wake model obtained by the superposition of Kaimal turbulence with Larsen model. Color bar in percentage; the downstream rotor circumference is indicated by a black circle.

on the wind farm layout and the wind direction in addition to wind speed. While the general problem of wake detection is very interesting and also quite important for wind farm control purposes, the attention is restricted in this work to the sole use of the information obtained by the proposed estimation technique.

A detection based on SEWS is investigated first. To this end, Fig. 9 shows various wake interference scenarios, defined by the lateral distance between the rotor centers of the upstream and downstream wind turbines, for an ambient mean wind speed of 8 m/s, a TI of 5% and a shear leayer with exponent equal to 0.2. For each scenario, corresponding to a column subplot of the overall figure, the left and right sector wind speed estimates are displayed as functions of time. Each column subplot also reports reference values computed by spatially averaging the wind speed at each instant of time from the synthetic turbulent wind field. Such reference values represent a ground truth with respect to which the estimates should be compared.

The figure clearly shows that in partial wake conditions (±0.75D, ±0.5D and ±0.25D) the SEWS is, as expected, smaller on the side of the rotor disk affected by the wake. This difference increases for increasing overlap, suddenly dropping to zero when the downstream rotor is in full wake condition. Clearly, any wind speed estimator can not readily distinguish between a full waked and a completely unwaked condition, although wind direction and wind farm layout may come to the help in such a case. Interestingly, the plot also shows that the estimates seem to follow quite well the ground truth, correctly identifying both the sign and the magnitude of the wind speed imbalance over the two rotor sides.

Based on these observations, a simple approach to detect a wake interference condition is to calculate the relative wind speed difference δ_{V} between the two rotor sides, by using a moving averaged SEWS calculated on the left and right quadrants:

$$\delta_{\mathrm{V}} = \frac{\bar{V}_{\mathrm{SE,left}} - \bar{V}_{\mathrm{SE,right}}}{\bar{V}_{\mathrm{RE}}}. \tag{17}$$

An indication of a left or right-sided wake impingement may be obtained by checking the sign of δ_{V} and

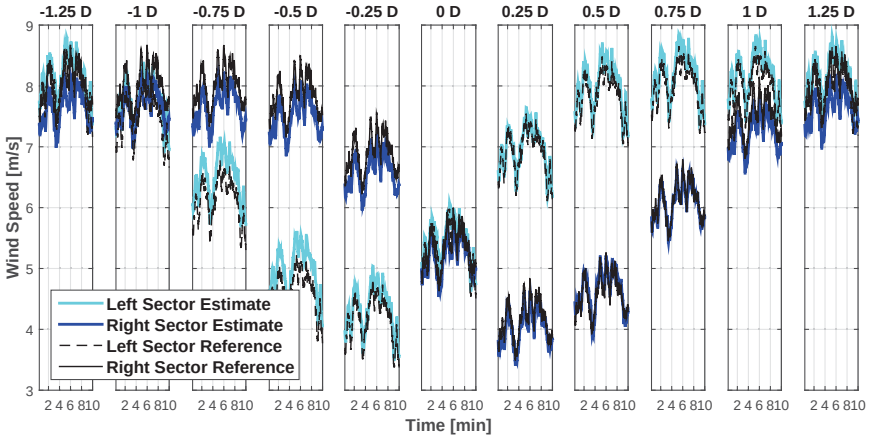

Figure 9: Estimated and reference (ground truth) sector wind speeds vs. time. Each column plot represents a different wake overlap, characterized by a different lateral distance between upstream and downstream rotor centers. Left sector SEWS: reference speeds shown in black dashed lines, estimates in cyan; right sector SEWS: reference speeds in black solid lines, estimates in blue.

comparing its absolute value with a threshold. It was observed that slightly different left and right thresholds could be used for better detection performance, on account of the non-symmetric lateral behavior of the rotor, due to its spin direction.

In turbulent unwaked wind conditions, speed fluctuations due to the passage of large eddies will generate significant lateral shears, which may be wrongly interpreted as the presence of a wake by the impingement detector. Similarly, in waked conditions, large turbulent fluctuations may temporarily hide the presence of the wake speed deficit. These problems may be alleviated by computing δ_V not with the instantaneous SEWS values, but with moving averages computed on a sufficiently long window of time to filter out the effects of turbulent fluctuations. Clearly, excessively long time windows would have the effect of inducing long delays and missing wake motions due to meandering.

In support of the information coming from wind speed imbalances, also TI can be used as an additional indicator of wake interference. Similarly to the previous plot, Fig. 10 shows the ground truth and estimated SETI values for different degrees of overlap between the two machines. Here again it appears that the proposed estimator is capable of appreciating the differences in TI over the two sides of the rotor. In addition, these estimates correlate quite well with their reference values. Consequently, one could here again define a relative TI difference δ_{TI}, exactly as done for the wind speed. Checking the value and magnitude of this additional indicator could be used for reinforcing the information obtained by computing the wind speed imbalance, in the interest of a hopefully more robust and reliable indicator.

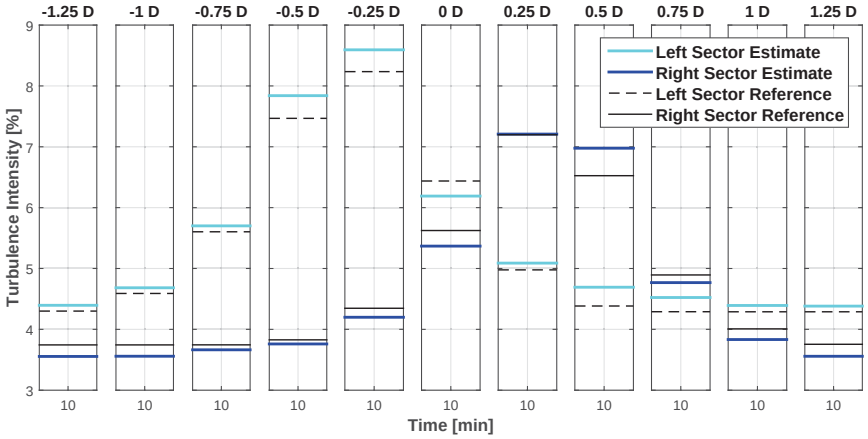

Figure 10: Estimated and reference (ground truth) sector TIs vs. time. Each column plot represents a different wake overlap, characterized by a different lateral distance between upstream and downstream rotor centers. Left sector SETI: reference TIs shown in black dashed lines, estimates in cyan; right sector SETI: reference TIs in black solid lines, estimates in blue.

4.4. Simulation studies

In the following, several wake interference scenarios were realized with the wind and turbine models described above. Wake detection was based in all cases on the δ_V parameter, therefore looking for an imbalance of the SEWS on the right and left quadrants of the rotor. The threshold in δ_V used for discriminating a wake interference from a non-interference case was set to 0.12, while the time span of the moving average window to 60 sec. Wind conditions also included a power-law vertical wind shear κ and downwind turbine yaw misalignment γ, to investigate the effects of these parameters on the detection quality.

Figure 11 shows results obtained for four different shear and turbulence intensity combinations. For different overlaps, each plot displays the detection ratio on the right quadrant (dark blue bars pointing upwards), and on the left one (light blue bars pointing downwards). The detection ratio is defined as the ratio of the number of time instants when the wake is detected, divided by the total number of time instant in a sequence of a given length (here chosen to be 10 min). For each combination of parameters, one single 10-minute sequence was used, as additional realizations lead only to marginal changes in the results.

For the cases of low ambient turbulence (TI=5%) with two different vertical shear layers, results show that a wake can be always detected for overlaps between around $0.25D$ and $0.75D$ on either side of the disk. For the cases characterized by higher ambient turbulence (TI=10%), the wake is not always perfectly detected due to a faster wake recovery, which in turn leads to a smaller wake deficit. In fact, the wake model predicts a maximum deficit in the wake center of around only 2.5 m/s. That deficit is not as large as in the low turbulence case, where the maximum deficit is about 4.5 m/s. This smaller deficit creates a smaller difference between SEWS on the two rotor sides, in turn decreasing the detection quality. However, the detection ratio

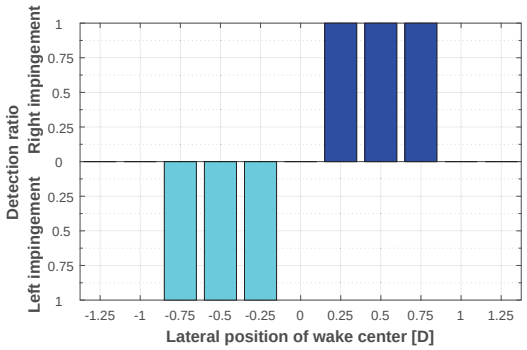

(a) $\kappa = 0.0$, $\gamma = 0$ deg, TI=5%

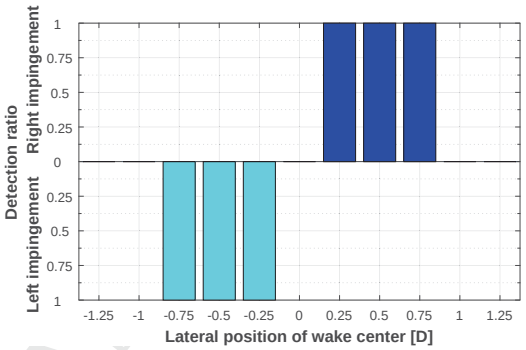

(b) $\kappa = 0.2$, $\gamma = 0$ deg, TI=5%

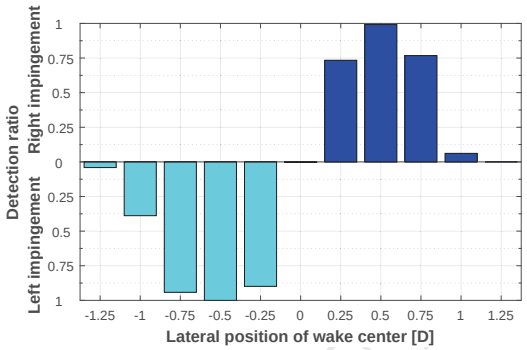

(c) $\kappa = 0.0$, $\gamma = 0$ deg, TI=10%

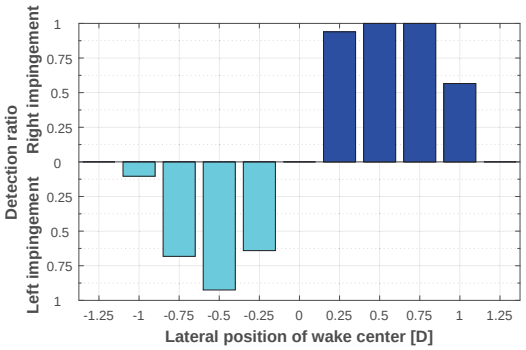

(d) $\kappa = 0.2$, $\gamma = 0$ deg, TI=10%

Figure 11: Wake state detection based on SEWS estimation for varying wake overlap, for an 8 m/s ambient wind speed and different vertical shear and ambient TI.

remains sufficiently high for all conditions between $0.25D$ and $075D$. It also appears that, although false negatives are clearly present, false positives are typically not. Improvement are foreseeable by scheduling both threshold and moving average window size as functions of ambient parameters, at the expense of an increased overall complexity of the algorithm implementation and use.

Figure 12 shows results for one single wind condition (vertical shear exponent equal to 0.2, TI=5%), but for four different yaw misalignment angles of the downstream wind turbine (γ=$\pm$10° and $\pm$20°). These conditions are meant to represent situations when the downstream wind turbine is actively redirecting its wake away from a machine located further downstream, using some suitable control strategy. In all cases the detection quality is similar to the non-misaligned case reported previously. This can be explained by the fact that the SEWS of the two lateral sectors are little affected by wind direction.

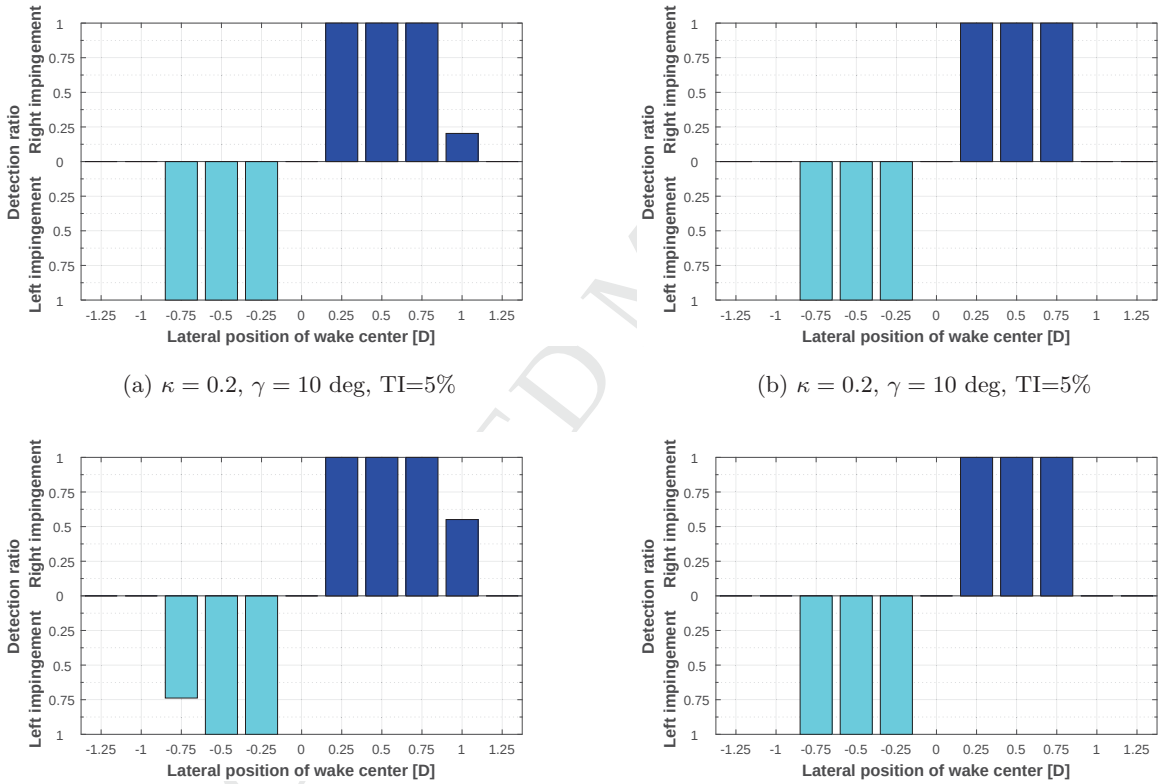

(a) $\kappa = 0.2$, $\gamma = 10$ deg, TI=5%

(b) $\kappa = 0.2$, $\gamma = 10$ deg, TI=5%

(c) $\kappa = 0.2$, $\gamma = -20$ deg, TI=5%

(d) $\kappa = 0.2$, $\gamma = 2$ deg, TI=5%

Figure 12: Wake state detection based on SEWS estimation for varying wake overlap and different misalignment of the downstream wind turbine, for an 8 m/s ambient wind speed, vertical shear exponent equal to 0.2 and TI=5%.

Next, a case characterized by a meandering wake was considered. In order to approximate such a case, the

lateral distance y between wake and turbine center was varied in time according to the following expression:

$$y = 1\mathrm{D}\big(\sin(2\pi f t) - 1\big), \tag{18}$$

where f is the meandering frequency. Accordingly, the resulting wake will oscillate between an unwaked state ($y = -2\mathrm{D}$) to a fully waked one ($y = 0\mathrm{D}$). In total, 28 wake oscillations with a frequency of $f = 0.05$ Hz were analyzed, for an ambient mean wind speed of 8 m/s, TI of 5% and a vertical shear layer exponent $\kappa = 0.1$. In this scenario, it is important to ensure a fast detection in order to capture wake motions. To this end, the detection threshold was raised to 0.2 and the moving average filter was eliminated. This same combination of parameters yields good results also in the low turbulence conditions analyzed earlier. The resulting detection ratio is displayed in Fig. 13.

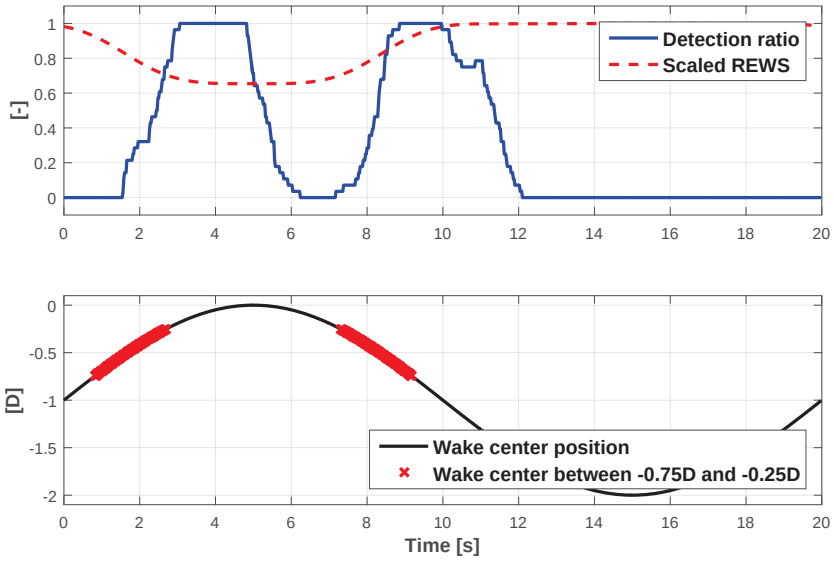

Figure 13: Upper subplot: detection ratio (blue line) for the meandering wake problem, and scaled REWS (dashed red line), as an average over 28 cycles. Lower subplot: wake center positions vs. time over one cycle.

The lower subplot shows the oscillating wake center. Positions between -0.75D and -0.25D are marked in red, since within that range a correct wake state detection is typically possible, as previously shown. The upper subplot shows the scaled mean REWS, using a dashed red line. This quantity was computed on the wind grid, and clearly exhibits a drop when a significant wake overlap is present.

The same upper plot also shows the detection ratio, using a solid blue line, which indicates that a left-sided wake impingement is detected twice throughout a full meandering cycle. When the wake center is far outside of the rotor disk, a wake impingement is never detected, so that there are no false positives. The first detection peak refers to the entrance of the wake on the rotor disk, while the second one to its exit,

both times on the left side of the rotor disk. The gap between these two peaks corresponds to the full wake condition, realized when the wake is exactly aligned in front of the downstream wind turbine. This situation could be perhaps detected by comparing the REWS on the upstream and downstream wind turbines, as well as considering the alignment of their connecting line with the wind direction. Comparing the detection rate with the wake center position, a delay of about 2 seconds can be observed. This time delay corresponds to approximatively 1/3 of a rotor revolution, and it is due to the fact that a new estimate of the SEWS is realized only once a blade leaves a sector.

5. Conclusions and outlook

This work has presented the formulation of a new method to estimate the wind speed inflow at the rotor disk of a wind turbine. The proposed method falls within the general area of wind sensing, where the whole rotor is turned into a sensor. By using measurements of the rotor response, in this case in the form of blade loads, the response is inverted to estimate the wind conditions. If load sensors are available on a wind turbine, for example to enable load-driven control, the present method does not require any additional hardware and it amounts to a simple software upgrade.

The proposed approach uses the cone coefficient, which captures the zeroth-harmonic bending of the blades, to infer the wind speed by means of a Kalman filter. When loads from all rotor blades are used together, a rotor-equivalent wind speed can be estimated. Simulation and experimental results shown here indicate that this method compares favourably with the well known approach based on the power coefficient. Furthermore, it also appears that the time resolution is sufficient to successfully estimate the associated RETI and REILS.

However, differently from other wind sensing approaches, the proposed formulation has also the ability of sensing variations of the wind speed over the rotor disk. In fact, by using the bending moment measured on each blade individually, one can obtain local estimates of the wind speed. These estimates were here averaged over four rotor quadrants, to yield sector-equivalent wind speed measurements.

The knowledge of areas of different local wind speeds over the rotor disk can be used to infer a lack of uniformity of the wind field. In particular, it was shown with the help of experimental field test data that the method is capable of observing the different wind speeds that characterize the top and bottom quadrants of the rotor, on account of the vertical shear profile.

As an even more interesting application, the paper considered also the detection of the impingement of the wake shed by an upstream wind turbine. Since a wake is characterized by a speed deficit and an increased TI, a partial wake overlap can in principle be detected by measuring speed and TI on the left and right quadrants of the rotor. Simulation results indicate that this is indeed possible with the proposed approach. In fact, studies conducted with a high-fidelity aeroservoelastic model of a wind turbine interacting with a

552 turbulent wake model have shown the general ability of the present method in detecting the presence of a
553 partial wake overlap, even in the presence of wake meandering.

554 The proposed idea is being further investigated along different lines of research. From a validation point
555 of view, the method is being demonstrated with the help of wind tunnel tests conducted with aeroelastically
556 scaled models. Full-scale experiments with LiDAR measurements of waked conditions should become available
557 soon, hopefully enabling a first verification in the field. Additionally, the scaled experimental facility is being
558 used for exploiting the proposed method at the wind farm control level, where it is being used to trigger a
559 left or right deflection of the upstream wake, based on where the wake impingement is detected. The method
560 is also being used to improve the quality of the estimates produced by a reduced order flow model, used for
561 closed-loop model-based wind farm control. Finally, the vertical resolution provided by the use of sectors is
562 being exploited for the identification of the presence of low level jets in the atmosphere.

563 **Acknowledgements**

564 The authors gratefully acknowledge Dr. Paul Fleming (NWTC, NREL) for having provided the CART3
565 experimental data.

566 [1] T. Knudsen, T. Bak, M. Svenstrup, Survey of wind farm control-power and fatigue optimization, Wind
567 Energy 18 (8) (2015) 1333–1351. doi:10.1002/we.1760.

568 [2] P. A. Fleming, P. M. O. Gebraad, S. Lee, J.-W. van Wingerden, K. Johnson, M. Churchfield, J. Micha-
569 lakes, P. Spalart, P. Moriarty, Evaluating techniques for redirecting turbine wakes using SOWFA, Re-
570 newable Energy 70 (2014) 211 – 218. doi:10.1016/j.renene.2014.02.015.

571 [3] A. Jiménez, A. Crespo, E. Migoya, Application of a LES technique to characterize the wake deflection
572 of a wind turbine in yaw, Wind Energy 13 (6) (2010) 559–572. doi:10.1002/we.380.

573 [4] J. Wang, S. Foley, E. M. Nanos, T. Yu, F. Campagnolo, C. L. Bottasso, A. Zanotti, A. Croce, Numerical
574 and experimental study of wake redirection techniques in a boundary layer wind tunnel, in: Wake
575 Conference, Visby, Sweden, 2017. doi:10.1109/acc.2011.5991022.

576 [5] F. Campagnolo, V. Petrovìc, J. Schreiber, E. M. Nanos, A. Croce, C. L. Bottasso, Wind tunnel testing
577 of a closed-loop wake deflection controller for wind farm power maximization, J. Phys.: Conf. Ser.
578 753 (032006). doi:10.1088/17426596/753/3/032006.

579 [6] P. M. O. Gebraad, F. C. van Dam, J.-W. van Wingerden, A model-free distributed approach for wind
580 plant control, in: American Control Conference (ACC), Washington, DC, USA, 2013, pp. 628–633.
581 doi:10.1109/acc.2013.6579907.

[7] J. Annoni, P. M. O. Gebraad, A. K. Scholbrock, P. A. Fleming, J.-W. van Wingerden, Analysis of axial-induction-based wind plant control using an engineering and a high-order wind plant model, Wind Energy. doi:10.1002/we.1891.

[8] Z. Yang, Y. Li, J. Seem, Individual pitch control for wind turbine load reduction including wake interaction, in: American Control Conference (ACC), Washington, DC, USA, 2011, pp. 5207–5212. doi:10.1109/acc.2011.5991022.

[9] P. M. O. Gebraad, F. W. Teeuwisse, J. W. van Wingerden, P. A. Fleming, S. D. Ruben, J. R. Marden, L. Y. Pao, Wind plant power optimization through yaw control using a parametric model for wake effects – a CFD simulation study, Wind Energy 19 (1) (2016) 95–114. doi:10.1002/we.1822.

[10] N. S. Ghaisas, C. L. Archer, Geometry-based models for studying the effects of wind farm layout, Journal of Atmospheric and Oceanic Technology. doi:10.1175/jtech-d-14-00199.1.

[11] H. Wang, R. J. Barthelmie, Wind turbine wake detection with a single Doppler wind LiDAR, Journal of Physics: Conference Series 625 (1) (2015) 012017. doi:10.1088/1742-6596/625/1/012017.

[12] M. Soltani, T. Knudsen, M. Svenstrup, R. Wisniewski, P. Brath, R. Ortega, K. Johnson, Estimation of rotor effective wind speed: a comparison, IEEE Transactions on Control Systems Technology 21 (4) (2013) 1155–1167. doi:10.1109/tcst.2013.2260751.

[13] C. L. Bottasso, C. E. D. Riboldi, Estimation of wind misalignment and vertical shear from blade loads, Renewable Energy 62 (2014) 293–302. doi:10.1016/j.renene.2013.07.021.

[14] C. L. Bottasso, C. E. D. Riboldi, Validation of a wind misalignment observer using field test data, Renewable Energy 74 (2015) 298 – 306. doi:10.1016/j.renene.2014.07.048.

[15] M. Bertelè, C. L. Bottasso, S. Cacciola, F. D. Adegas, S. Delport, Wind inflow observation from load harmonics, Wind Energy Science under review.

[16] C. L. Bottasso, S. Cacciola, F. Campagnolo, J. Schreiber, Wake detection for wind farm control – formulation and validation, in: AIAA Scitech, San Diego, CA, USA, 2016, p. 1741, doi:10.2514/6.2016-1741.

[17] S. Cacciola, M. Bertelè, J. Schreiber, C. Bottasso, Wake center position tracking using downstream wind turbine hub loads, J. Phys.: Conf. Ser. 753 (032036). doi:10.1088/1742-6596/753/3/032036.

[18] J. Schreiber, S. Cacciola, F. Campagnolo, V. Petrovìc, D. Mourembles, C. L. Bottasso, Wind shear estimation and wake detection by rotor loads — first wind tunnel verification, J. Phys.: Conf. Ser. 753 (032027). doi:10.1088/1742-6596/753/3/032027.

[19] R. P. Coleman, A. M. Feingold, Theory of self-excited mechanical oscillations of helicopter rotors with hinged blades, Tech. Rep. TN 1351, NACA (1958).

[20] K. Z. Østergaard, P. Brath, J. Stoustrup, Estimation of effective wind speed, in: Journal of Physics: Conference Series, Vol. 75, IOP Publishing, 2007, p. 012082.

[21] X. Ma, N. Poulsen, H. Bindner, Estimation of wind speed in connection to a wind turbine, Tech. rep., Informatics and Mathematical Modelling, Technical University of Denmark (1995).

[22] C. L. Bottasso, A. Croce, Advanced control laws for variable-speed wind turbines and supporting enabling technologies, Tech. rep., Dipartimento di Ingegneria Aerospaziale, Politecnico di Milano (January 2009).

[23] I. Munteanu, G. Besançon, Control-based strategy for effective wind speed estimation in wind turbines, in: IFAC'14, 19th World Congress of the International Federation of Automatic Control, Cape Town, South Africa, 2014, pp. 6776–6781. doi:10.3182/20140824-6-ZA-1003.01952.

[24] J. F. Manwell, J. G. McGowan, A. L. Rogers, Wind Energy Explained, John Wiley & Sons, Ltd, 2009. doi:10.1002/9781119994367.

[25] C. L. Bottasso, A. Croce, Cp-Lambda users's manual, Tech. rep., Dipartimento di Scienze e Tecnologie Aerospaziali, Politecnico di Milano (2006–2016).

[26] O. A. Bauchau, C. L. Bottasso, L. Trainelli, Robust integration schemes for flexible multibody systems, Computer Methods in Applied Mechanics and Engineering 192 (34) (2003) 395 – 420. doi:10.1016/S0045-7825(02)00519-4.

[27] N. D. Kelley, B. J. Jonkman, Overview of the TurbSim stochastic inflow turbulence simulator, Tech. rep., National Renewable Energy Laboratory (February 2007).

[28] P. A. Fleming, A. D. Wright, L. J. Fingersh, J.-W. van Wingerden, Resonant vibrations resulting from the re-engineering of a constant-speed 2-bladed turbine to a variable-speed 3-bladed turbine, in: 49th AIAA Aerospace Sciences Meeting, Orlando, FL, USA, 2011, pp. 4–7. doi:10.2514/6.2011-634.

[29] J. M. Jonkman, An aeroelastic computer-aided engineering (CAE) tool for horizontal axis wind turbines, NWTC Information Portal (FAST), https://nwtc.nrel.gov/FAST. Last modified 19-March-2015; Accessed 02-February-2016 (2015).

[30] J. M. Jonkman, M. L. Buhl, FAST user's guide. 6.0 ed. (2005).

[31] D. J. Renkema, Validation of wind turbine wake models, Master's thesis, Delft University of Technology (2007).

Research Highlights

- New method to estimate wind speed based on load measurements, turns the rotor into a wind sensor.
- Differently from other methods, the present approach can detect *local* wind speed variations over the rotor disk.
- The paper demonstrates the new method for the estimation of the vertical wind shear and the impingement of the wake of an upstream wind turbine.
- The new wake detector is shown to reliably estimate the wake location over the rotor disk, showing promise for its use in wind turbine and wind farm control.